

**Experimental characterization of damage during geothermal production of hot dry rocks
Comprehensive effects of the damage-elastic deformation on conductivity evolution**

Xu, Fuqiang; Shi, Yu; Song, Xianzhi; Wu, Wei; Song, Guofeng; Li, Shuang

DOI

[10.1016/j.energy.2024.130871](https://doi.org/10.1016/j.energy.2024.130871)

Publication date

2024

Document Version

Final published version

Published in

Energy

Citation (APA)

Xu, F., Shi, Y., Song, X., Wu, W., Song, G., & Li, S. (2024). Experimental characterization of damage during geothermal production of hot dry rocks: Comprehensive effects of the damage-elastic deformation on conductivity evolution. *Energy*, 294, Article 130871. <https://doi.org/10.1016/j.energy.2024.130871>

Important note

To cite this publication, please use the final published version (if applicable).
Please check the document version above.

Copyright

Other than for strictly personal use, it is not permitted to download, forward or distribute the text or part of it, without the consent of the author(s) and/or copyright holder(s), unless the work is under an open content license such as Creative Commons.

Takedown policy

Please contact us and provide details if you believe this document breaches copyrights.
We will remove access to the work immediately and investigate your claim.

Green Open Access added to TU Delft Institutional Repository

'You share, we take care!' - Taverne project

<https://www.openaccess.nl/en/you-share-we-take-care>

Otherwise as indicated in the copyright section: the publisher is the copyright holder of this work and the author uses the Dutch legislation to make this work public.



Experimental characterization of damage during geothermal production of hot dry rocks: Comprehensive effects of the damage-elastic deformation on conductivity evolution

Fuqiang Xu ^a, Yu Shi ^{b,*}, Xianzhi Song ^a, Wei Wu ^c, Guofeng Song ^d, Shuang Li ^a

^a College of Petroleum Engineering, China University of Petroleum (Beijing), Beijing, China

^b Faculty of Geosciences and Environmental Engineering, Southwest Jiaotong University, Chengdu, China

^c School of Civil and Environmental Engineering, Nanyang Technological University, Singapore

^d Department of Geoscience and Engineering, Delft University of Technology, Delft, the Netherlands

ARTICLE INFO

Handling Editor: Prof G Iglesias

Keywords:

Hot dry rocks
Injection experiment
Conductivity evolution
Fracture damage
Elastic deformation
Comprehensive effects

ABSTRACT

The development of hot dry rocks (HDRs) is of great significance to adjusting energy structure, alleviating energy shortage, reducing pollution, etc. Low-permeability granite is the predominant rock type in deep HDRs, making fractures the primary pathways for fluid circulation and heat extraction. The production of HDRs is significantly influenced by variable fracture conductivity, but current conductivity characterization primarily relies on the elastic deformation of the matrix, neglecting the impact of damage. Accordingly, we propose an experimental method and a supporting apparatus, which is used to unveil the conductivity evolution characteristics resulting from the comprehensive effects of damage and elastic deformation. The experimental results demonstrate that when subjected to confining force squeezing inward, the fracture conductivity experiences varying degrees of decrease compared to its initial state before the experiment. By utilizing the conductivity evolution rate as the evaluation criterion and conducting grey correlation analysis, it has been determined that temperature exerts the most significant influence on the conductivity evolution, followed by injection flow, and lastly, confining pressure. Moreover, rock particle types and production cycles also have different degrees of effect. After considering the comprehensive effects of damage-elastic deformation at the field-scale, the damage has a positive effect on conductivity enhancement. Our study provides a new approach for the characterization of fracture conductivity evolution for deep geothermal projects.

1. Introduction

Geothermal resources are renewable, sustainable, environmentally friendly, and abundant natural resources. Among these resources, HDR geothermal reservoirs play a pivotal role, characterized by high temperatures and substantial reserves [1]. Granite is a common type of HDR which is dense [2,3], so the enhanced geothermal system (EGS) is the main method for the development of HDRs, and the natural fractures and hydraulic fracturing fractures are the main flow-heat transfer channels for working fluids [4–7].

Previously, the fracture conductivity is usually regarded as a constant during thermal exploitation. However, the fluid injection will cause the rock to shrink significantly due to the change in pore pressure and temperature, that is, elastic deformation [8,9]. Moreover, the

temperature drop caused by fluid injection will also cause rock damage, such as fracture propagation, weak cementation failure, micro-crack germination particle spalling, etc [10,11]. Elastic deformation and damage together affect changes in conductivity [11]. Understanding the fracture conductivity evolution of fractured rocks is of great significance, such as designing/adjusting production scenarios of HDRs, preventing/reducing the generation of micro-seismic in the mining process, etc [12–14].

Compared with elastic deformation, the effect of damage on the conductivity evolution is currently not systematic, because the types of damage are diverse, and it is difficult to characterize. Uneven heating or cooling is the main reason for rock damage, because granites are complex mixtures of multiple minerals with significant differences in thermodynamic properties [15,16]. More works have been conducted

* Corresponding author.

E-mail address: shiyu@swjtu.edu.cn (Y. Shi).

<https://doi.org/10.1016/j.energy.2024.130871>

Received 6 August 2023; Received in revised form 1 January 2024; Accepted 29 February 2024

Available online 7 March 2024

0360-5442/© 2024 Elsevier Ltd. All rights reserved.

concerning the variations in the properties of granite after heating and various subsequent cooling methods (e.g., cooled in air, liquid nitrogen, oven, or water) [11,17–19]. There are five major factors affecting the characteristics of thermal damage [20,21], namely (1) temperature difference, (2) heating and cooling rate, (3) thermal history, (4) degree of mineralogy heterogeneity, and (5) stress conditions. For the mining process of the HDRs, the first item mainly corresponds to the temperature of the circulating fluid and the rock matrix, especially the temperature difference between the two [22,23]. The second term corresponds to the cooling rate of the rock after encountering the cold fluid, which is mainly related to the size of injection flow and convection heat transfer coefficient, etc [17,24]. The third mainly corresponds to the production mode, such as continuous and intermittent, the difference between the two is that the latter has a process of reservoir temperature recovery, and the rock will undergo “fatigue damage” under repeated cooling [18,25]. The fourth item mainly corresponds to the difference in thermodynamic and mechanical properties of the mineral composition of the rock [26,27]. The fifth item mainly corresponds to the force of the rock in the formation, which will affect the rock strength and stress field distribution, and then affect the threshold of rock damage and the direction of fracture extension [11], more, it also affects the fracture aperture.

In terms of the rock samples used in the experiment, the existing cooling method is mainly to cool the rock sample as a whole [28–30], which is essentially different from the injection water in the fractures (local cold zone) in HDR mining [11]. Of course, many scholars have carried out research on the fracture morphology and the conductivity evolution [10,23,31–33]. Shu et al. [31,32] developed a custom-designed high-temperature fluid flow-through device and analyzed the effect of confining pressure and temperature on the hydraulic and heat extraction characteristics of single fractures in granite samples (ϕ 50 mm \times 100.0 mm and ϕ 50 mm \times 300.0 mm). The metrics they used for evaluation were equivalent hydraulic aperture, permeability, and hydraulic conductivity. Li et al. [23] developed a fracture conductivity testing system, and they used granite samples (ϕ 25.4 mm \times 60.0 mm) containing fracture (split) to analyze the temperature-dependent mechanical properties of hydraulic fracture surfaces and their influence on conductivity. They mainly used fracture conductivity to evaluate the experimental results. Guo et al. [10] designed a hydraulic fracturing and seepage simulator, and they used the granite cores (ϕ 25.0 mm \times 50.0 mm) containing fracture (split) to carry out experiments on the evolution of fracture conductivity. The metrics they used for evaluation were injection pressure and permeability retention rate. Zhang et al. [33] used convective heat transfer simulation equipment and granite samples (ϕ 50 mm \times 100.0 mm) to study the evolution process of different morphologies of rock fractures under high temperature and high pressure, and their evaluation indicators mainly include aperture and permeability.

Existing research provides research ideas for the experimental acquisition of fracture conductivity, however, there are still the following areas that need to be supplemented and improved: (1) Experimental temperature is usually below 200 °C, and most hot dry rock reservoirs exceed this value; (2) The impacts of damage on the evolution of fracture conductivity are not thoroughly investigated across multiple parameters, and the relative importance of each parameter remains unclear; (3) The evolution of fracture conductivity under the combined influences of elastic deformation and damage is not well-understood.

Therefore, the current research is organized as follows: **Section 2** introduces the rock samples, experiment apparatus, and procedure; **Section 3** discusses the effects of damage on the conductivity evolution under multiple parameters corresponding to the five main factors that cause thermal damage; **Section 4** compares the affected priority of different parameters on damage, and the fracture damage characteristics are analyzed; Finally, **Section 5** summarizes the main conclusions of the present work. In addition to the development of HDRs geothermal, the

research also contributes to other high-temperature underground rock engineering projects, such as geological disposal of nuclear waste, geological sequestration of CO₂, and shale gas development, etc.

2. Methods and materials

2.1. Experimental apparatus

To precisely assess changes in conductivity, a multi-field coupling experimental platform for rock core injection and mining has been designed and developed. The apparatus utilizes natural or artificial fracture rock samples and conducts fluid seepage-heat transfer experiments within fractures. Key components of the apparatus comprise a clamping device, heater, constant flow pump, temperature-controlling device, and data acquisition system, as depicted in Fig. 1(a). The maximum axial and confining pressures are loadable up to 55 MPa and 50 MPa, respectively. It can be set by the computer's automatic loading function, with constant pressure, tracking, and other control modes, and can be loaded axial or confining pressure separately. The flow pressure in the device ranges from 0 to 30 MPa, and the injection flow is controllable within the range of 0.1–60 ml/min. Pressure and temperature sensors boast accuracies of 0.001 MPa and 0.01 °C, respectively, fulfilling the real-time measurement requirements of the experiment. The system has a maximum temperature resistance of 350 °C, making it suitable for a majority of conditions encountered in underground high-temperature engineering experiments.

The most important component of the experimental apparatus is the clamping device, as shown in Fig. 1(b). The clamping device adopts a special structural design that can achieve high-temperature and high-pressure sealing: First, the initial sealing is achieved by applying a flexible graphite gasket, high-temperature resistant silicone material, and sealant; Then, when the axial pressure and confining pressure are applied, the self-tightening gasket actively compresses the graphite gasket, and the higher the pressure, the better the sealing performance. After pre-experimental testing, effective sealing can still be achieved at a temperature of 300 °C and a stress difference of 15 MPa. It fully meets the needs of the rock seepage test under various high-temperature conditions.

The data acquisition system is also an important component of the apparatus. The whole apparatus is controlled and collected by computer, as shown in Fig. 2 (red dashed line). It can realize all-around monitoring and control, real-time acquisition, and data processing of system instrument parameters. High-precision sensors are installed at the injection and extraction ends of rock samples and can monitor temperature and pressure in real-time. In addition to the devices shown in the figure, the instruments used in the experiment include the muffle furnace, and CT (computed tomography), as shown in Fig. 3, which are used for rock sample heating (pretreatment), fracture shape and volume change comparison and analysis, respectively. The resolution of the CT device can reach less than 40 μ m in terms of experimental rock sample size, and the maximum design heating temperature of the muffle furnace chamber can reach 1100 °C [11]. The above apparatus can fully meet the needs of the experiment.

2.2. Rock samples

Outcrop rock samples obtained from Laizhou, Shandong Province, China, according to the size of rock particles, can be divided into two types: coarse-grained granite and fine-grained granite. The mineral composition and physical properties of granites are shown in Table 1 [11]. The diameter of the cylindrical fracture rock sample used for experiments is 100 mm, and the length is 200 mm (\pm 5 mm). The selection criteria for rock samples are as follows: The fracture penetrates the rock and splits the rock almost symmetrically into two parts, and the two parts can be well combined. All rock samples are prepared from the same granite with natural fractures, except for coarse-grained rock samples, as

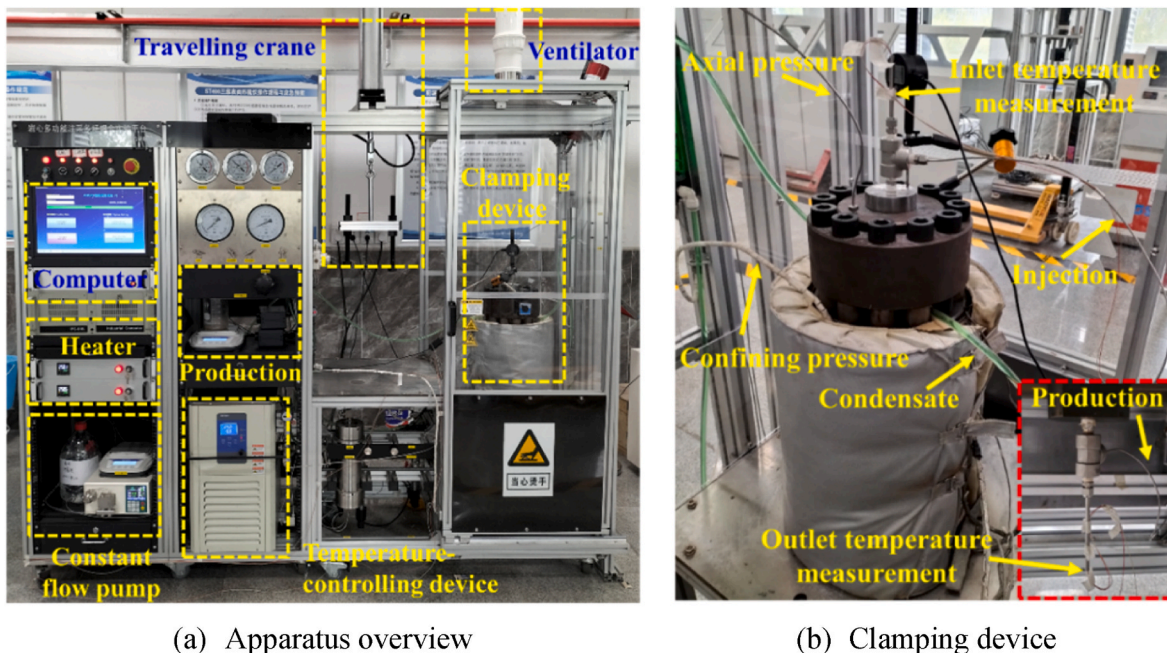


Fig. 1. Multi-field coupling experimental platform for fluid injection and mining.

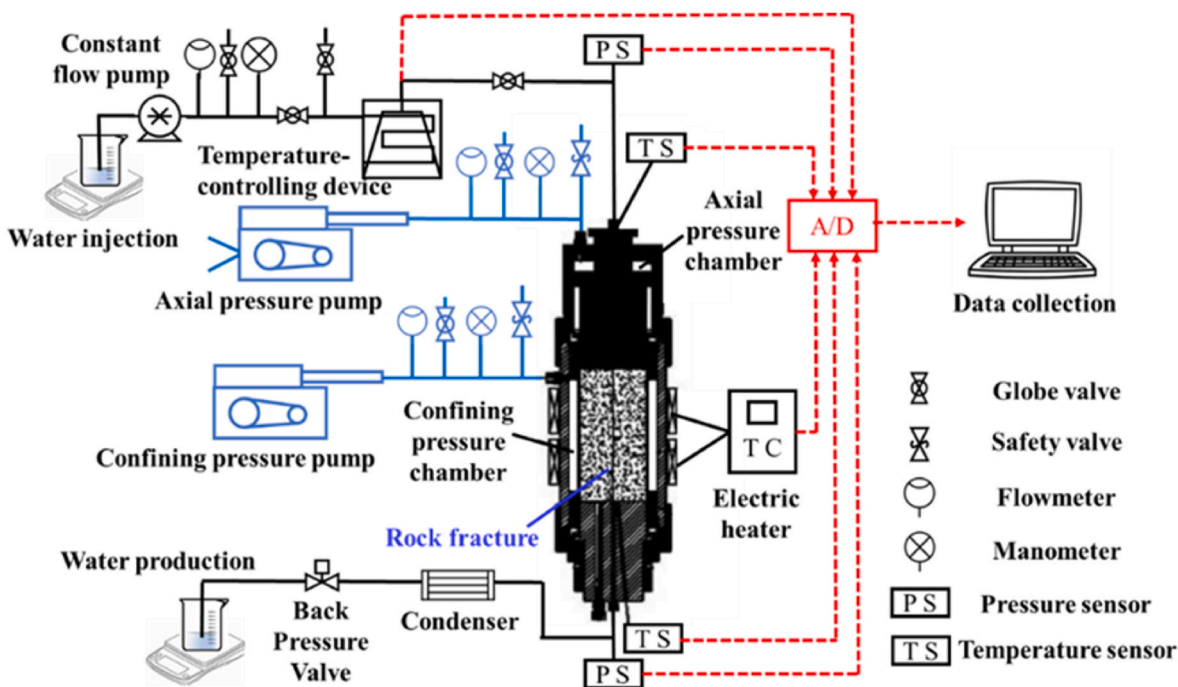


Fig. 2. Schematic diagram of the experimental platform.

shown in Fig. 4(a) and Fig. 4(b). Moreover, for ease of understanding, if it is not specifically described later, the granite mentioned is fine-grained granite.

The preparation and pretreatment of rock samples include the following processes: First, it is heated in the muffle furnace and then cooled to room temperature in the furnace chamber. The heating rate is 1.5 °C/min, and after heating to the specified temperature, it is kept heat preserved for 1 h. The above process needs to be repeated three times, to minimize the effect of thermal damage during the heating and cooling process. Then, the fracture surface is cleaned and washed with water and an air gun, to remove the loose particles; Finally, the split rock sample is

reassembled into the whole, and its outer wall is successively coated with high-temperature sealant, thread seal tape, and the high-temperature silicone sleeve (interference fit), to ensure that the fluid can only flow in the fracture, as shown in Fig. 4(c).

2.3. Experimental procedure

The experimental procedure is shown in Fig. 5. After completing the rock sample preparation and pretreatment (as mentioned in Section 2.2), the rock sample is placed in the clamping device shown in Fig. 2 (b), and the experimental apparatus is assembled. Testing the fracture's

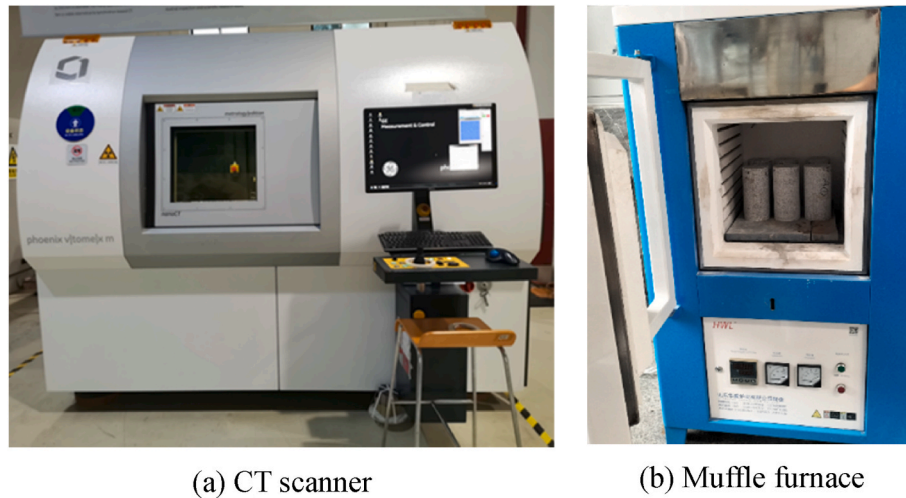


Fig. 3. CT scanner and muffle furnace.

Table 1

Mineral composition and physical properties of fine-grained and coarse-grained granite [11].

Items (Fine-grained granite)	Value	Items (Coarse-grained granite)	Value
Density, g/cm ³	2.63	Density, g/cm ³	2.64
Tensile strength, MPa	8.79	Tensile strength, MPa	9.20
Elastic modulus, GPa	58.95	Elastic modulus, GPa	54.16
Poisson's ratio	0.243	Poisson's ratio	0.241
Compressive strength, MPa	553.0	Compressive strength, MPa	425.7
Shear strength, MPa	301.5	Shear strength, MPa	287.6
Fine-grained granite:		Coarse-grained granite:	
Quartz 39.0%; Plagioclase 35.2%;		Quartz 36.9%; Plagioclase 36.7%;	
Orthoclase 12.3%; Augite 8.0%;		Orthoclase 12.1%; Iron mica 6.3%;	
Clay mineral 2.8%; Glauberite 2.7%		Ferrodolomite 5.1%; Glauberite 2.9%	

initial conductivity at room temperature, denoted k_1 . It should be noted that the experiment obtains a differential pressure, and its conversion relationship with the conductivity will be given later. Then, the rock sample is heated to the experimental temperature at the same heating rate as the rock sample pretreatment and kept heat preserved. After the rock sample is heated uniformly, cold water is injected into the fracture, and the production pressure is set to 2 MPa. After the temperature of the produced water is stable, continue to inject water for a period of time to simulate the actual production process of HDRs. Then, the heating and water injection are stopped, and the sample is cooled to room temperature for the same cooling time as the sample pretreatment. Finally, test the fracture conductivity of superimposed damage at room temperature, denoted k_2 . To be clear, the scale of the rock samples used is small, and the injection-mining parameters are scaled by equal proportions. Therefore, although the experiment time is short (tens of minutes), it can be considered a long-term production for this experiment.

During the above experiments, the temperature of the rock sample changed significantly, as shown in Fig. 6. Start heating from point *a* to point *b* of the experimental temperature, and it is kept heat preserved to equalize the temperature of the rock sample. Cold fluid is injected at point *c*, and the temperature of the water produced at point *d* begins to drop, indicating that the thermal breakthrough occurs. As the heat source continues to replenish heat, the temperature of the water produced at point *e* reaches a constant value, and the water injection continues to be maintained. Finally, stop heating and water injection at point *f*, and wait for the rock to cool to room temperature (point *g*). It should be noted that the length and slope of the curve in Fig. 6 do not represent numerical size, but are only used to represent a certain stage.

The experimental protocols are shown in Table 2. The parameters studied include rock sample temperature (temperature difference),

injection flow (heating/cooling rate), axial and confining pressure (stress difference), rock particle type (mineralogy heterogeneity), and continuous/intermittent mining (thermal history), corresponding to the five main causes of thermal damage to rocks mentioned in Section 1. Among them, the parameters of the basic scheme are set as follows: rock sample temperature 280 °C, injection temperature 20 °C, injection flow 4 ml/min, production pressure 2 MPa, axial pressure, and confining pressure of 20 MPa and 10 MPa, respectively. The parameter settings of the basic scheme are presented in parentheses in Table 2. In parameter studies, research parameters are modified on the basic scheme, and other settings are the same, as shown in Table 2.

Moreover, the flow rate in this test is quite small, so Darcy's law of fluid flow can be used to calculate the conductivity (product of permeability and aperture, denoted k , m²·m) of a single fracture [34], and it can be expressed as follows [23,35]:

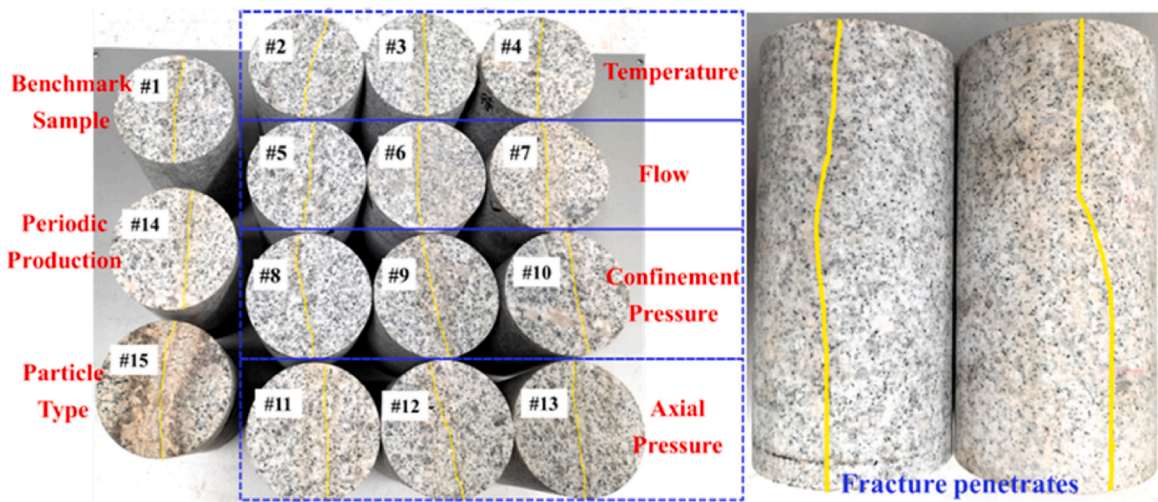
$$k = \frac{Q\mu L}{D_s \omega (p_{in} - p_{out})} \quad (1)$$

Rock samples are obtained from the same rock, and their specifications are the same, so the change value in injection-mining pressure difference (Δp) can be used to compare the changes in the conductivity in combination with the above equation, that is, the larger the pressure difference, the smaller the corresponding fracture conductivity. Moreover, the current research primarily focuses on analyzing the evolution of damage over time, whereas this study aims to analyze the effects of multiple parameters on damage. Recognizing the irreversibility of the damage process, multiple rock samples are used to experiment, and the analysis employs the conductivity evolution rate (ke) to mitigate the impact of rock heterogeneity on the results, as follows:

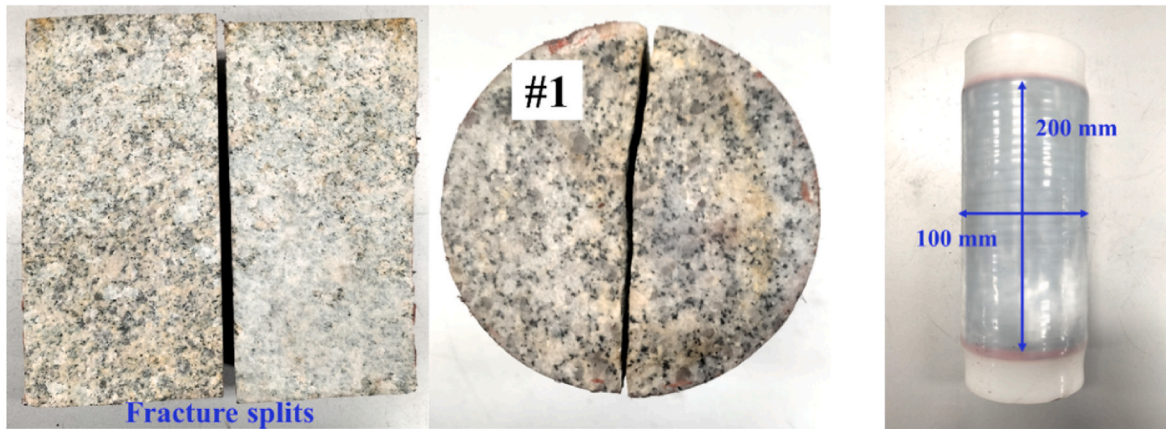
$$\Delta p = \Delta p_{after} - \Delta p_{before} \quad (2)$$

$$ke = \left(\frac{Q\mu L}{D_s \omega \Delta p_{after}} - \frac{Q\mu L}{D_s \omega \Delta p_{before}} \right) / \left(\frac{Q\mu L}{D_s \omega \Delta p_{before}} \right) \times 100\% \\ = \left(\frac{\Delta p_{before}}{\Delta p_{after}} - 1 \right) \times 100\% \quad (3)$$

where Q (m³/s) is the injection rate, μ (Pa·s) is the viscosity of water, D_s (m) and L (m) are the diameter and length of core samples, respectively, ω (m) is the fracture aperture, p_{in} (Pa) and p_{out} (Pa) are the injection and production pressures, Δp_{before} (Pa) and Δp_{after} (Pa) are the pressure difference measured before and after the experiment, which is used to represent k_1 and k_2 in Fig. 5, respectively.



(a) Rock samples for experiments (no splitting)



(b) Fracture view (splitting)

(c) Jacketed samples

Fig. 4. Rock samples required for the experiment.

3. Experimental results

3.1. Stress difference

Rocks are subjected to in-situ stress in the original occurrence environment and are in a state of equilibrium, but the stress in all directions is generally different. The anisotropy of in-situ stress has an important influence on the direction of micro-crack germination and damage degree, which further affects the fracture conductivity. Therefore, experiments under different confining and axial pressures are carried out to analyze the influence of diverse stress differences on the conductivity evolution.

Axial pressure is always greater than or equal to the confining pressure during the experiment, and the fracture surface is almost perpendicular to the confining pressure direction, that is, perpendicular to the direction of the minimum principal stress, which is consistent with the actual situation.

During the experiment, with the injection of cold fluid, the stress field disturbance will occur inside the rock, especially near the fractures, and the expression of the effective stress change is as follows [36]:

$$\sigma_e = \frac{\sigma_1 + \sigma_2 + \sigma_3}{3} + \alpha_B p \quad (4)$$

where, σ_e (Pa) is the effective stress, Pa, σ_1 , σ_2 and σ_3 (Pa) represent the principal stresses, α_B is the Biot-Willis coefficient, and p (Pa) is the pore

pressure.

Fracture penetrates and evenly divides the rock sample, as shown in Fig. 4, and there is always a set of confining pressures in the direction of the normal direction of the fracture. From Fig. 7, with the increase of confining pressure, the pressure difference shows a clear upward trend, and the law all exists before and after the experiment. For example, comparing the injection-mining pressure difference at 5 MPa and 20 MPa, the value is 0.564 MPa (Δp_{before}) before the experiment and 0.765 MPa (Δp_{after}) after the experiment. The initial fracture aperture is about the same, and there are differences in the degree of fracture closure under different confining pressures, that is, a large confining pressure corresponds to a small fracture aperture, and a small aperture corresponds to large flow resistance and high-pressure difference.

The above laws are found by comparing the data before and after the experiment under different confining pressures. The Δp under 5 MPa, 10 MPa, 15 MPa, and 20 MPa of confining pressure are 0.228 MPa, 0.201 MPa, 0.344 MPa and 0.429 MPa, respectively. There are many reasons for the above phenomenon, such as chemical precipitation-dissolution, rock particle blockage, damage causing aperture change, etc. The time scale is relatively small and the chemical reaction is not violent, and the rock is split from natural fractures and is in close contact under confining pressure, making it difficult for the peeling particles to move. Therefore, the main reason for the above phenomenon is the failure of the support caused by the damage, which in turn leads to the fracture closure.

The pressure difference increases, which is mainly caused by the

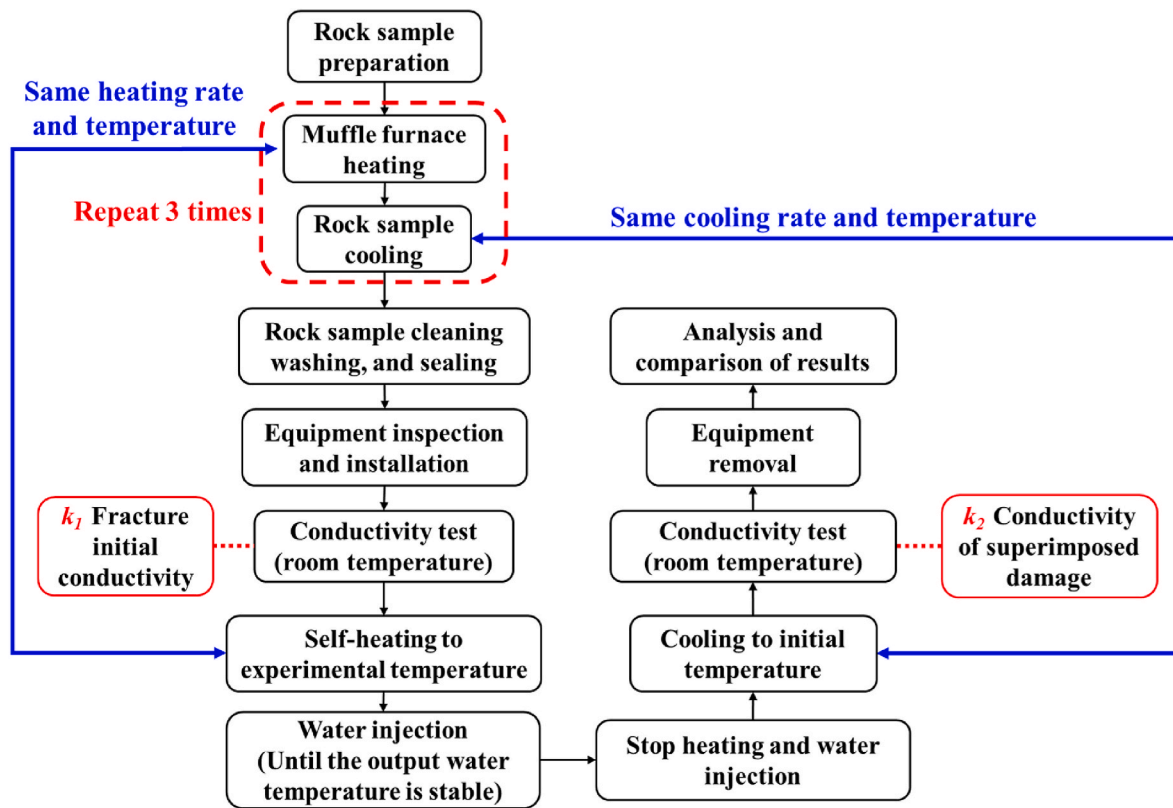


Fig. 5. Experimental procedure for characterization.

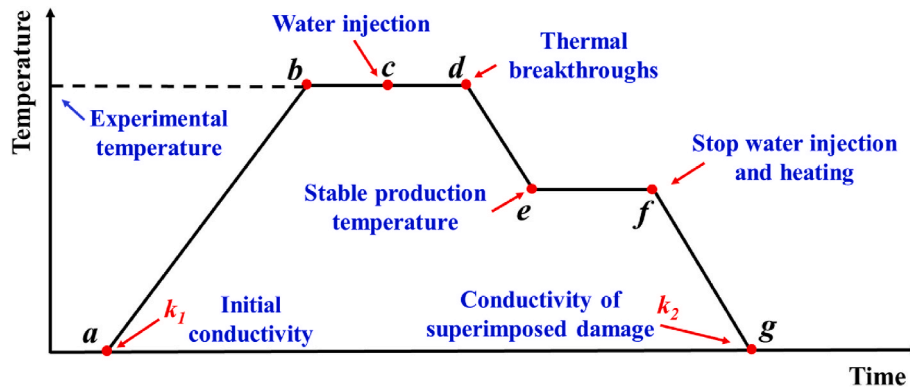


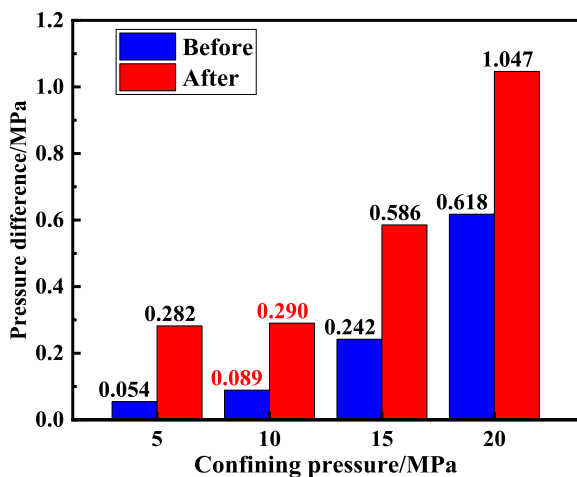
Fig. 6. Rock sample heating and cooling procedure.

Table 2
Experimental scheme.

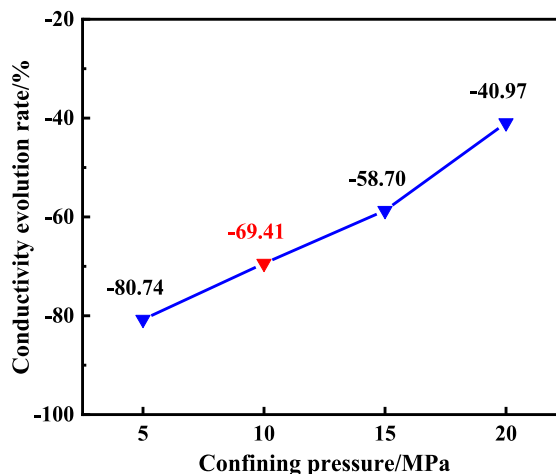
Experiment Type	Parameters	Value Range
Basic scheme (1 groups)	Temperature (280 °C), Injection flow (4.0 ml/min), Axial pressure- Confining pressure (20 MPa–10 MPa), Particle type (Fine), Periodic production (Continuous)	
Parameter evaluation experimental design (14 groups)	Temperature, °C	190, 220, 250, (280)
	Injection flow, ml/min	2.0, (4.0), 6.0, 8.0
	Axial pressure, MPa	15, (20), 25, 30
	Confining pressure, MPa	5, (10), 15, 20
	Rock particles type	(Fine), Coarse
Periodic production	(Continuous), Intermittent	

failure of particle support at the fracture, resulting in the decrease of fracture aperture. The fracture surface is not a smooth plane, but a rough surface, and there are a lot of point-to-point supports [35]. With the fluid injection, the stress field inside the rock, especially near the fractures, changes under the action of thermal stress and pore pressure [11]. Pore pressure and thermal stress are tensile stresses, which are opposite to the compressive stress caused by the confining pressure, and when the stress at a point in the rock changes from compressive stress to tensile stress, and exceeds the tensile limit of that point, the rock will be damaged. The fracture is the main channel for fluid flow and heat exchange, and the temperature drop near the fracture is the greatest during the development of HDRs, and the particles at the fracture are loosely cemented, so the fracture is the location where the initial failure occurs.

The change value in injection-mining pressure difference at high confining pressure is greater, which can indicate that the small aperture is more sensitive to damage. More, in Section 2.3, it defines the



(a) Pressure difference



(b) Conductivity evolution rate

Fig. 7. Pressure difference and conductivity evolution rate vary with confining pressure.

conductivity evolution rate (ke), which changes with the confining pressure as shown in Fig. 7(b), as the confining pressure increases, the absolute value of ke gradually decreases, and presents a nearly linear relationship, from 80.74% at 5 MPa to 40.97% at 20 MPa, and the absolute value decreases by 39.77%. The above law indicates that the damage degree is greater at low confining pressure. According to Eq. (4), under small confining pressure, the fracture is subjected to less compressive stress at the initial moment. The larger the confining pressure, the greater the value of pore pressure, but the change amplitude is small, as shown in Fig. 7(a). The tensile stress is mainly caused by thermal stress under the experimental conditions of this paper. The smaller the initial compressive stress, the less difficult and easier it is to achieve the force at the fracture from compressive stress to tensile stress.

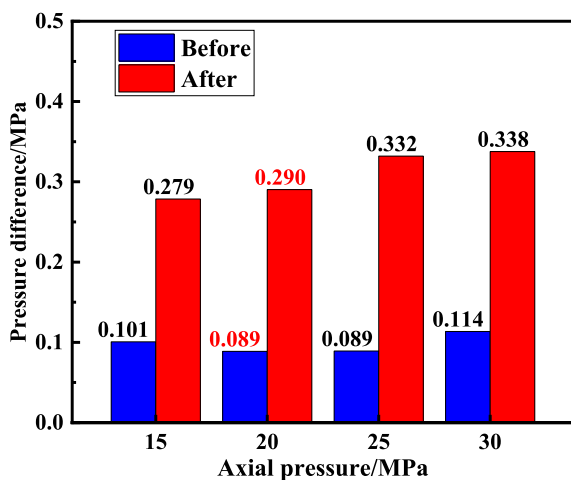
Under the research conditions in this paper, the influence of axial pressure change on fracture conductivity is not significant, as shown in Fig. 8. The Δp (ke) under 15 MPa, 20 MPa, 25 MPa, and 30 MPa of axial pressure are 0.178 MPa (-63.84%), 0.201 MPa (-69.41%), 0.243 MPa (-73.10%) and 0.224 MPa (-66.38%), respectively. The primary reasons are as follows: (1) The axial pressure direction does not align with the fracture closure/opening direction, leading to an indirect impact on the fracture aperture; (2) The influence of rock heterogeneity obscures the effect of axial pressure changes on damage; (3) The axial dimension

of the rock is greater than the radial direction, resulting in stronger resistance to deformation. In future research, further investigation will be conducted by modifying the experimental apparatus and adjusting the experimental protocol.

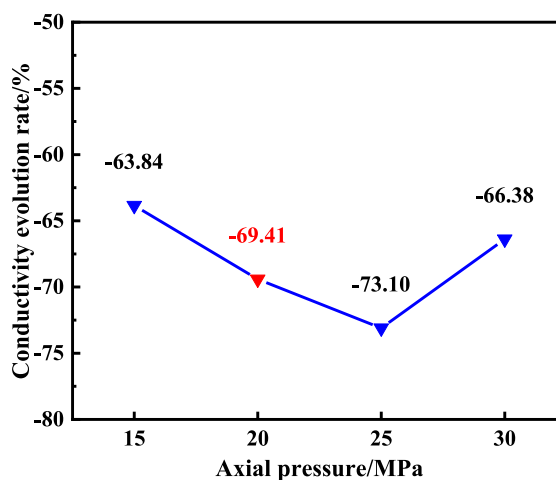
3.2. Injection flow

For a defined reservoir, injection flow is the most important controllable parameter and has an important impact on HDR production. From Fig. 9(a), the pressure difference increases with the increment of injection flow, which is caused by the changes in flow resistance, and it has been extensively demonstrated in previous studies. Moreover, the pressure difference after the experiment is significantly larger than the pressure difference before the experiment. When the flow is increased from 2 ml/min to 8 ml/min, the injection-mining pressure (Eq. (2)) changed orderly by 0.141 MPa, 0.201 MPa, 0.373 MPa, and 0.512 MPa, indicating that the conductivity is reduced to varying degrees after the experiment according to Eq. (1).

Section 3.1 has analyzed that the conductivity evolution is mainly caused by support failure. When other parameters are the same, a large injection flow means that there is more cold fluid to exchange heat with the rock matrix, the temperature drop near the fracture is greater, the



(a) Pressure difference



(b) Conductivity evolution rate

Fig. 8. Pressure difference and conductivity evolution rate vary with axial pressure.

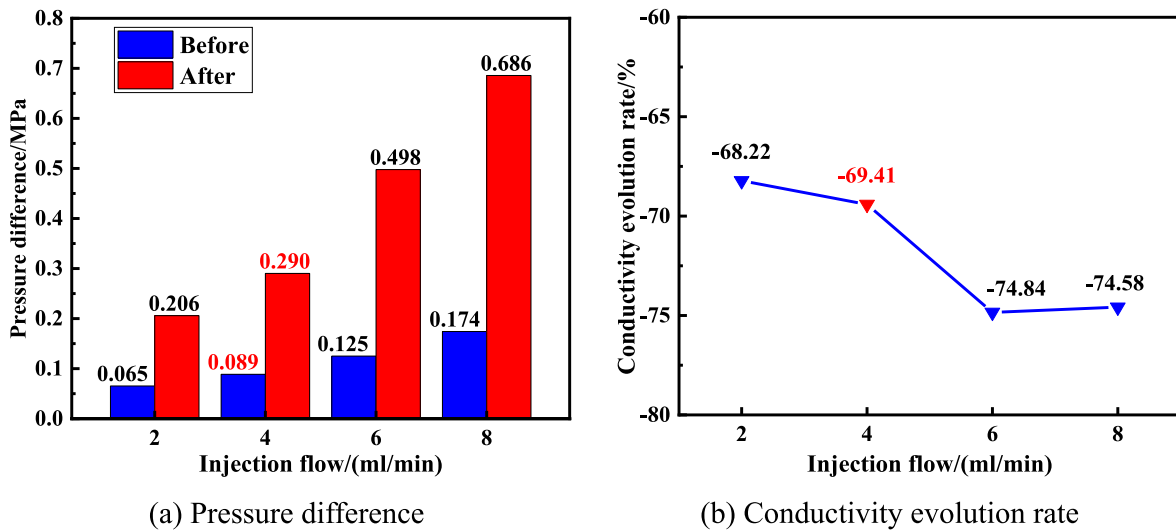


Fig. 9. Pressure difference and conductivity evolution rate vary with injection flow.

temperature gradient is more pronounced, and thermal stress is more likely to occur. In addition, the pore pressure is greater at large injection flow. The generation of the thermal stress and the change of pore pressure will intensify the process of changing the stress inside the rock from compressive stress to tensile stress (Eq. (4)), causing tensile failure of the rock.

The conductivity evolution rate in Fig. 9(b) further illustrates the above laws, that is, the damage degree is more pronounced under large injection flow. However, the degree of damage growth tends to stabilize at high injection flow, which may be due to the threshold of the impact of increased injection flow on damage. Because the main way that flow affects the evolution of conductivity is to change the temperature gradient, which is consistent with previous studies [11,23,37,38].

3.3. Temperature difference

Reservoir temperature is one of the important criteria for the selection of HDR targets. The temperature of Geysers EGS in the United States can reach 400 °C, the temperature of HDR in Qinghai Gonghe in China reaches 236 °C, and the target temperature of Bouillante in France, Lardarello in Italy, Coso and Newberry in the United States, and Cooper Basin in Australia are also above 200 °C [39], which are the high-grade

geothermal resource. Therefore, the research temperature in this paper is about 200 °C and above.

Influenced by rock heterogeneity, the pressure difference fluctuated greatly before the experiment, but the variation of pressure difference and the corresponding evolution rate of conductivity are obvious. From Fig. 10, compared with low temperatures, the amount and degree of rock damage increased significantly at high temperatures. The Δp (k_e) under 190 °C, 220 °C, 250 °C, and 280 °C of rock initial temperature are 0.127 MPa (-58.83%), 0.139 MPa (-64.68%), 0.181 MPa (-67.73%) and 0.201 MPa (-69.41%), respectively. The above law once again shows that the influence of thermal stress caused by temperature change on the conductivity evolution cannot be ignored. The curve in Fig. 10(b) also gradually flattens with the increase in temperature, indicating that after reaching a certain temperature, the change of rock damage degree decreases, and there is a temperature threshold for damage, which is consistent with previous studies.

3.4. Particle type and periodic production

Granite is the main type of HDR, and the particle size, mineral composition, and cementation degree of different granites are different, which directly causes distinct mechanical properties of rocks. In this

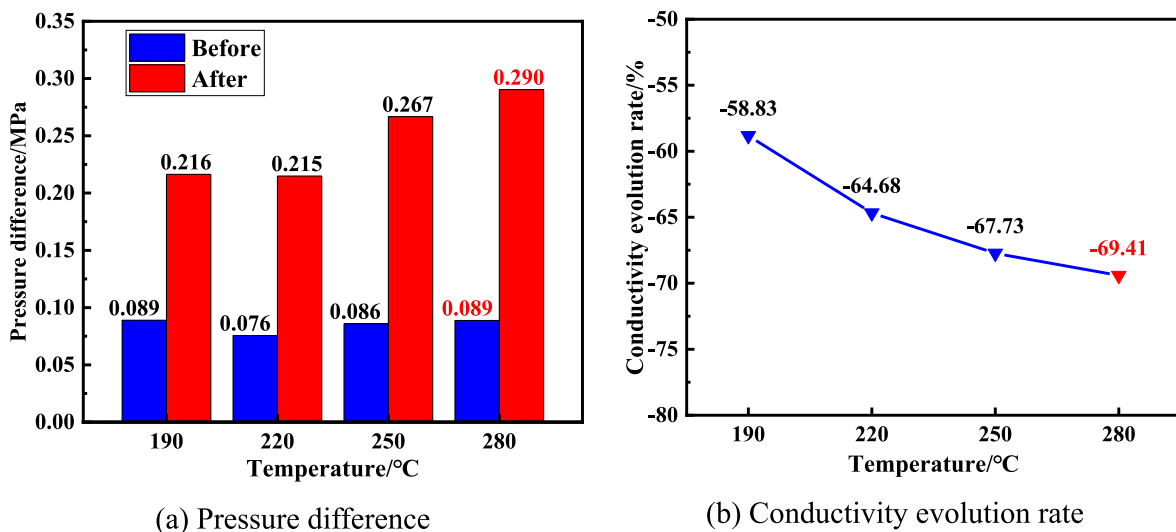


Fig. 10. Pressure difference and conductivity evolution rate vary with temperature.

paper, fine-grained granite and coarse-grained granite are selected for comparative experiments, and the mineral composition and physical properties of the rocks are shown in Table 1. From Fig. 11, the Δp of coarse-grained granite is 0.395 MPa, while the pressure difference value of fine-grained granite is only 0.201 MPa, and the former changed nearly twice as much as the latter. In addition, the conductivity evolution rate of coarse-grained granite is -82.93% , and the absolute value of the conductivity evolution rate is 13.52 percentage points larger than that of fine-grained granite (-69.41%). Coarse-grained granite is more susceptible to damage because it has a softer rock texture and less cementation at fractures than fine-grained granite, as shown in Fig. 4.

In the early stage of geothermal energy development, continuous production is mostly adopted, which can obtain more heat in a short time, but it will cause the heat breakthrough time to be advanced, and the heat production is low in the middle and late stages. Intermittent mining is proposed to realize reservoir temperature recovery and a higher production temperature [40]. The intermittent production in this paper refers to stopping water injection after the thermal breakthrough, heating the rock to experimental temperature, and then injecting water again, and the above process is cycled three times, as shown in Fig. 11 (a).

The Δp of intermittent production is 0.289 MPa, and the value of pressure difference change is 0.088 MPa larger than that of continuous production (0.201 MPa). Moreover, the conductivity evolution rate of intermittent production is -75.08% , and the absolute value of k_e is 5.67% larger than that of continuous production (-69.41%). The biggest difference between intermittent production and continuous production is that the former always maintains a high-temperature

gradient near fractures, which induces obvious thermal stress. Under intermittent production, multiple damage occurs to the rock, and the damage is a gradual accumulation process, which again shows that thermal stress has a significant effect on damage (conductivity evolution). Under the study conditions herein, the influence of different rock types on the conductivity evolution is more significant than that of production mode, as shown in Fig. 11(b) and (c).

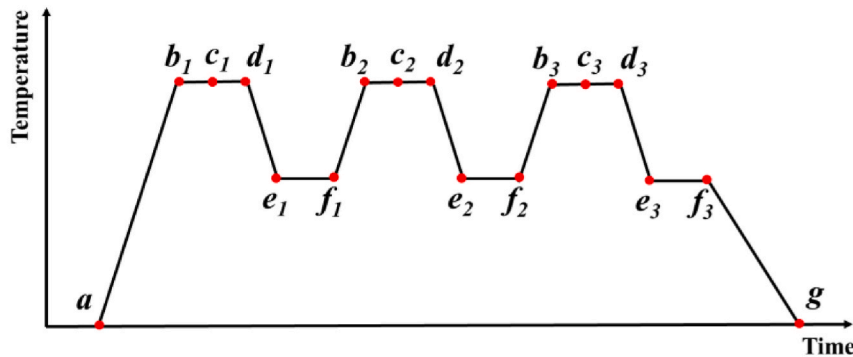
4. Discussion

4.1. Parameter importance analysis

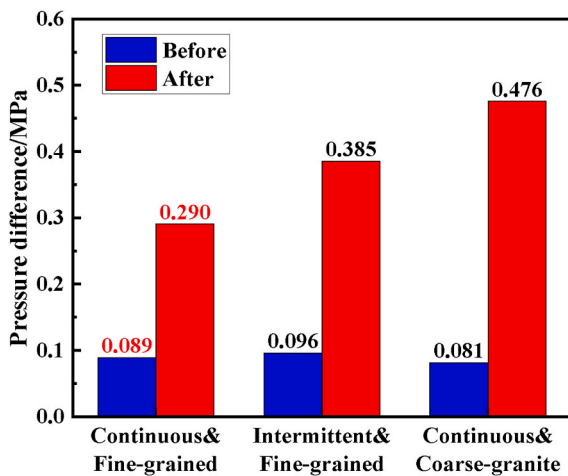
Based on the findings presented in Section 3, the degree of change in damage varies across the studied parameters, that is, the influence of each factor on the conductivity evolution has a priority. In this paper, three parameters exhibiting a clear pattern of effect on conductivity evolution are selected for evaluation: temperature, injection flow, and confining pressure, respectively.

The grey correlation analysis method is used to evaluate the parameter sensitivity. The method is to analyze the correlation between the factors of the system by comparing the similarity between the geometric relationship of the data series and the geometric shape of curves [41]. Its steps are as follows:

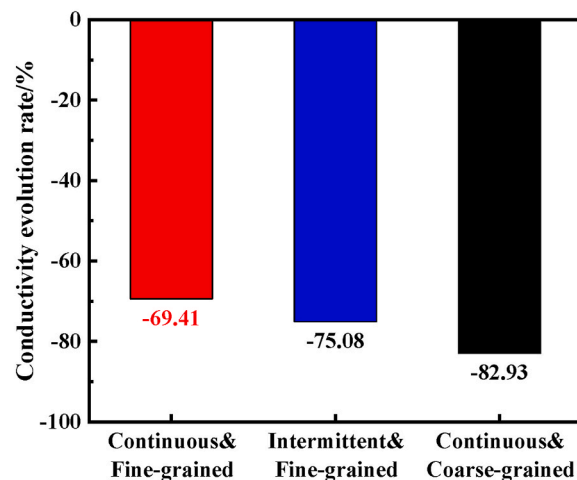
First, determine the series corresponding to the evaluation criteria and parameters [42]:



(a) Heating and cooling curve for intermittent production (Modified from Fig. 6)



(b) Pressure difference



(c) Conductivity evolution rate

Fig. 11. Heating-cooling process for periodic production; pressure difference and conductivity evolution rate vary with particle type and periodic production.

$$[X'_1 \ X'_2 \ \dots \ X'_n] = \begin{bmatrix} x'_1(1) & x'_2(1) & \dots & x'_n(1) \\ x'_1(2) & x'_2(2) & \dots & x'_n(2) \\ \vdots & \vdots & & \vdots \\ x'_1(m) & x'_2(m) & \dots & x'_n(m) \end{bmatrix} \quad (5)$$

$$X'_0 = (x'_0(1), \ x'_0(2), \ \dots \ x'_0(m))^T \quad (6)$$

where, X'_1 , X'_2 , and X'_3 represent the series corresponding to temperature, injection flow, and confining pressure, respectively. X'_0 represents the series corresponding to evaluation criteria. Considering the rocks' heterogeneity, different initial values may have a greater impact on the injection-mining pressure difference (Δp), resulting in inconspicuous or even inaccurate prioritization results, so a change value in conductivity evolution rate (ke) is used as the evaluation criterion in this paper.

Then, the data are dimensionless to exclude the influence caused by the difference of each index unit and the difference between their numerical orders of magnitude, and it uses the averaging method to process the data, that is, use of the average value of elements in all series as the divisor [43]:

$$x_i(k) = \frac{x_i(k)}{\frac{1}{n+1} \sum_{j=0}^n x_j(k)} \quad (7)$$

where $i = 0, 1, 2, \dots, n$ and $k = 1, 2, \dots, m$.

Next, calculate the Grey Relation Coefficient $\gamma(x_0(k), x_i(k))$ and Grey Relation Grade $\Gamma(x_0, x_i)$ [43]:

$$\gamma(x_0(k), x_i(k)) = \frac{\Delta_{\min} + \zeta \Delta_{\max}}{\Delta_{0,i}(k) + \zeta \Delta_{\max}} \quad (8)$$

$$\Gamma(x_0, x_i) = \sum_{k=1}^n \beta_k \gamma(x_0(k), x_i(k)), \quad \sum_{k=1}^n \beta_k = 1 \quad (9)$$

where $\Delta_{0,i}(k) = |x_0(k) - x_i(k)|$ is the difference of the absolute value between $x_0(k)$ and $x_i(k)$; $\Delta_{\min} = \min_{v,j} \min_{v,k} |x_0(k) - x_j(k)|$ is the smallest value of $\Delta_{0,j} \forall j \in \{1, 2, \dots, n\}$; $\Delta_{\max} = \max_{v,j} \max_{v,k} |x_0(k) - x_j(k)|$ is the largest value of $\Delta_{0,j} \forall j \in \{1, 2, \dots, n\}$; and ζ is the distinguishing coefficient, $\zeta \in (0, 1]$, expressed as the contrast between the background and the object to be tested, set to 0.5 in this paper, and β_k is the normalized weight for point k .

Finally, rank the relevance and draw conclusions. The correlation degree between temperature and ke is 0.879, and the values are 0.782 and 0.759 at injection flow and confining pressure, respectively, as shown in Fig. 12. Under the research conditions in this paper, the temperature has the greatest influence on ke , followed by injection flow, and finally confining pressure, which is roughly consistent with the previous law analysis.

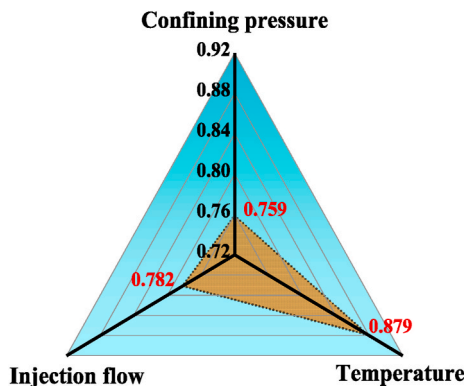


Fig. 12. Correlation degree between each parameter and the change value in ke .

4.2. Visual damage analysis

The fracture conductivity evolution is affected by both elastic deformation and damage. Water injection is carried out at high temperatures, and once the rock is damaged (fracture face point-to-point supports failure), the fracture will close under the confining pressure and the extrusion of the silicone sleeve (as shown in Fig. 4(c)). Even if the water injection is stopped and the rock is cooled to room temperature in the later stage, the rock undergoes elastic deformation (matrix shrinkage), but considering the outer force extrusion inward and the limited size of the rock sample, the fracture cannot open again, that is, the reduction in the conductivity caused by the damage is irreversible, and the similar law is drawn from the predecessors [35].

However, the volume of rock matrix in the actual reservoir is large, and the shrinkage deformation of rock cooling is much greater than the matrix deformation of indoor experiments. A large number of preliminary studies have shown that with the mining of HDRs, the temperature of the rock matrix near the fracture continues to decrease, and the fracture aperture increases significantly under the action of elastic deformation [1,36]. In addition, experiments are also carried out to verify this rule in this paper. CT scanning is used to compare fracture morphology before and after the experiment. To facilitate the identification of CT equipment, the rock sample is 35 mm in diameter and 60 mm in height (scanning height is 30 mm down from the injection end), and the constant flow pump in Fig. 1(a) is used for fluid pumping, other experimental conditions as follows: no confining pressure, no silicone sleeve sealed, the experimental temperature is about 300 °C, and the injection flow is 1.0 ml/min.

After water injection, the CT scan view of the fracture changed significantly, as shown in Fig. 13. In the scheme of no confining force extrusion, the fracture aperture, that is, the fracture conductivity increases. Crack propagation, cementation destruction, and micro-crack germination can be observed in the figure after the experiment. At this point, the damage increases the conductivity, which is achieved under the action of elastic deformation. In summary, during the actual mining of HDRs, elastic deformation, and damage will increase the fracture conductivity.

In Section 3, the influence of different parameters on the evolution of fracture conductivity is discussed, and it is concluded that damage will lead to a decrease in conductivity under experimental conditions in this paper. The main way of damage is still the failure of point-to-point support between fracture surfaces. The temperature drop near the fracture is large, and it is easy to damage in a short time, resulting in support failure, at which time the matrix is not sufficiently cooling and shrinking, so the fracture is temporarily closed, as shown in Fig. 14(b). However, the elastic deformation will increase the fracture aperture, so as long as the aperture increases to a certain value, the peeling particles will be carried out by the circulating working fluid, so the damage will eventually promote the increase of the fracture conductivity. The morphological changes of the fractures in the above process are shown in Fig. 14(c).

To analyze further the influence of damage on the conductivity evolution considering the actual elastic deformation at the reservoir scale, all rock samples used in Table 2 are selected for re-experiment. The rock sample treatment process is as follows: first, the silica gel sleeve, sealant, and other materials on the outside of the rock sample are removed; Then, the air gun is used to wash the peeled particles on the fracture surface and collect the particles; Finally, the rock sample is sealed and the differential pressure is measured again according to the same parameters as in the first experiment, like Fig. 4(c).

The rock sample at this time has a slightly wider aperture than the pre-first experiment, which is caused by particle spalling (removal). Fig. 15 shows the collected peeling particles, which can reach a maximum length of 5 mm and are in the form of sheets, indicating that the cementation of this part is relatively loose, and most of the peeling particles are less than 1 mm. The weight of the peeling particles varies

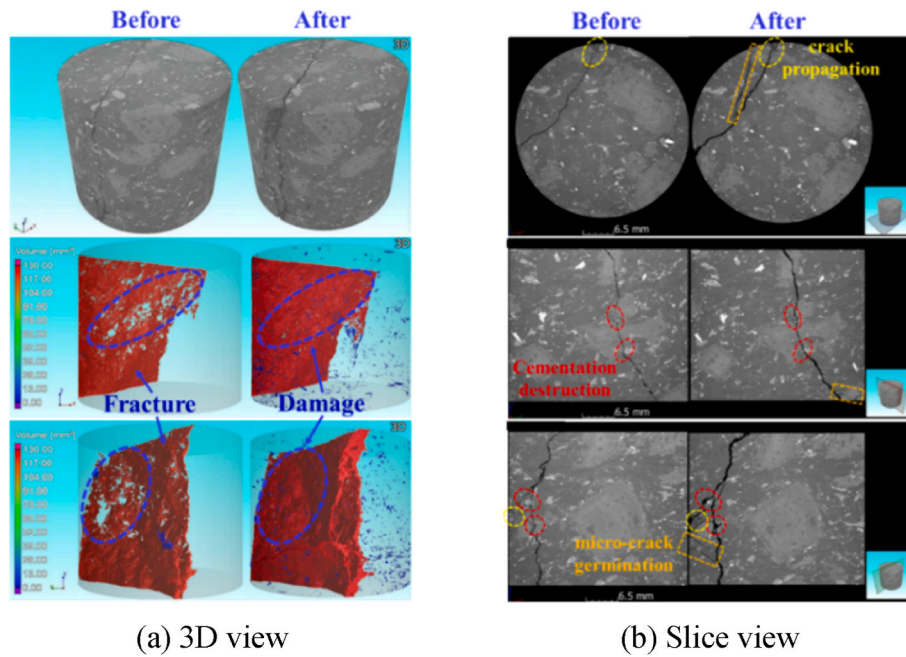


Fig. 13. CT scan view before and after the water injection.

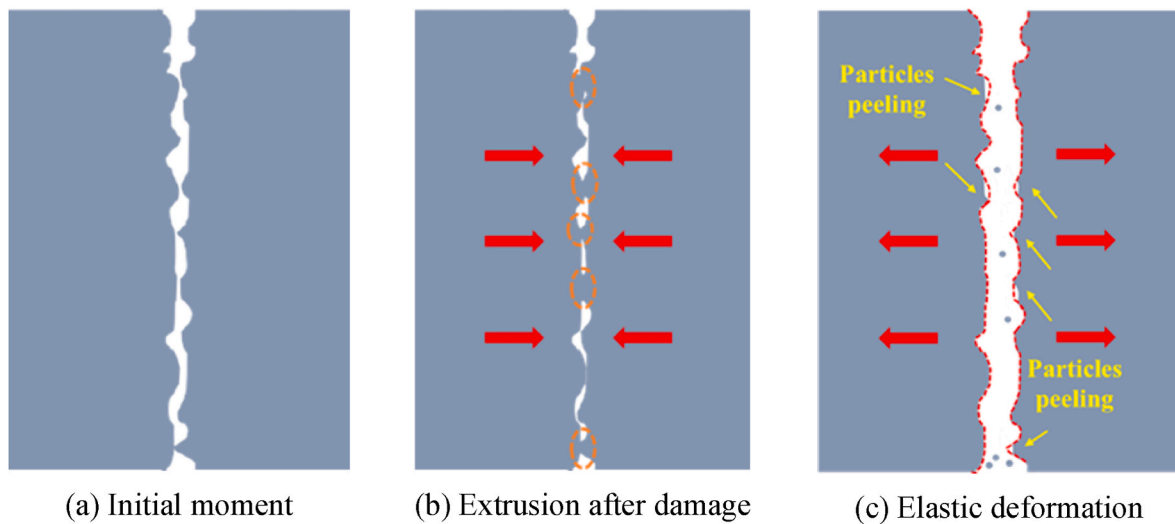


Fig. 14. Morphological changes of the fractures.

from 0.04 g to 0.32 g. Different types of particles peel off differently, which have been described in previous studies [11].

At this point, the expression of the change value in injection-mining pressure difference (Δp) and conductivity evolution rate (ke) are as follows:

$$\Delta p = \Delta p_{second} - \Delta p_{first} \quad (10)$$

$$ke = \left(\frac{Q\mu L}{D_s \omega \Delta p_{second}} - \frac{Q\mu L}{D_s \omega \Delta p_{first}} \right) \bigg/ \left(\frac{Q\mu L}{D_s \omega \Delta p_{first}} \right) \times 100\% \quad (11)$$

$$= \left(\frac{\Delta p_{second}}{\Delta p_{first}} - 1 \right) \times 100\%$$

where, Δp_{first} (Pa) and Δp_{second} (Pa) are the pressure difference measured before the first and second experiments, respectively.

From Fig. 16, after the peeling particles are removed, the pressure difference decreased to varying degrees compared with before the first

experiment, indicating that the conductivity increased. For example, with the increase of flow, the change amplitude is constantly rising, which corresponds to the law obtained in Section 3.2, that is, the damage increases with the increment of flow, and after considering the actual elastic deformation effect of the rock matrix, the damage can increase the fracture conductivity, which is mainly achieved by increasing the fracture aperture, as shown in Fig. 14(c). The confining pressure and temperature also follow the above-mentioned pattern, as shown in Fig. 16(b) and (d). Similarly, the magnitude of Δp and ke under coarse-grained granite and intermittent production is greater than in the basic scheme (continuous & fine-grained), as shown in Fig. 17, and the influence of rock particle type is greater than that of production mode, which is consistent with the law obtained in Section 3.4.

The above analysis shows that the damage caused in the first experiment has an increasing effect on the increase of fracture conductivity in the second experiment, and the greater the damage effect, the more obvious the amplitude of improvement.

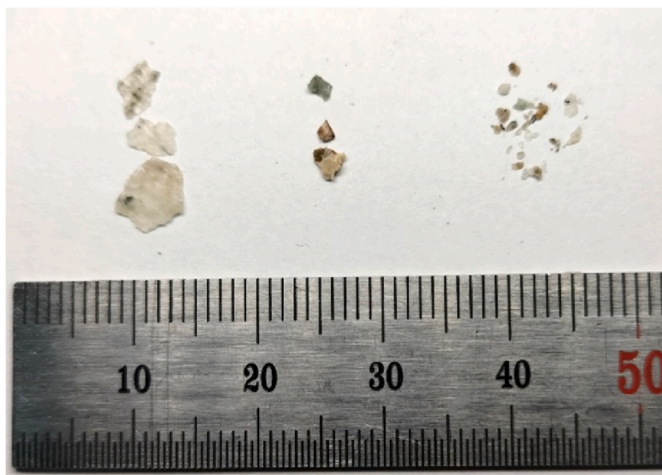


Fig. 15. Peeling rock particles (partial).

5. Conclusion

We designed and implemented a multi-field coupling experimental platform for conducting experiments on conductivity evolution. Through analysis of the experimental results, we examined the characteristics and mechanisms of fracture damage on the evolution of conductivity. Furthermore, we discussed the effects of fracture damage on conductivity evolution under various parameters. The key conclusions

are as follows.

- ✓ Considering only damage and confining force squeezing inward, the fracture conductivity after the experiment has different degrees of decrease compared with that before the experiment, which is caused by the rock damage. Crack propagation, weak cementation destruction, micro-crack germination, and particle spalling are the main modes of rock damage.
- ✓ By using grey relational analysis, the effect of temperature on the conductivity evolution is greater than injection flow, and the effect of confining pressure is minor. Particle type and production method also have a significant impact, and the effect of the former is more important.
- ✓ Considering the comprehensive effects of damage and elastic deformation in the geothermal reservoir, and conducting repeated experiments, the fracture conductivity shows varying degrees of increase, which increases with the enhancement of the damage degree, and it is explained experimentally.
- ✓ The study highlights a new approach for the test and analysis of fracture damage effect on conductivity evolution, which may contribute to high-temperature underground rock engineering projects. The experimental equipment and procedures need to be further retrofitted to improve the universality and accuracy of deep rock engineering research.

CRediT authorship contribution statement

Fuqiang Xu: Data curation, Methodology, Writing – original draft.

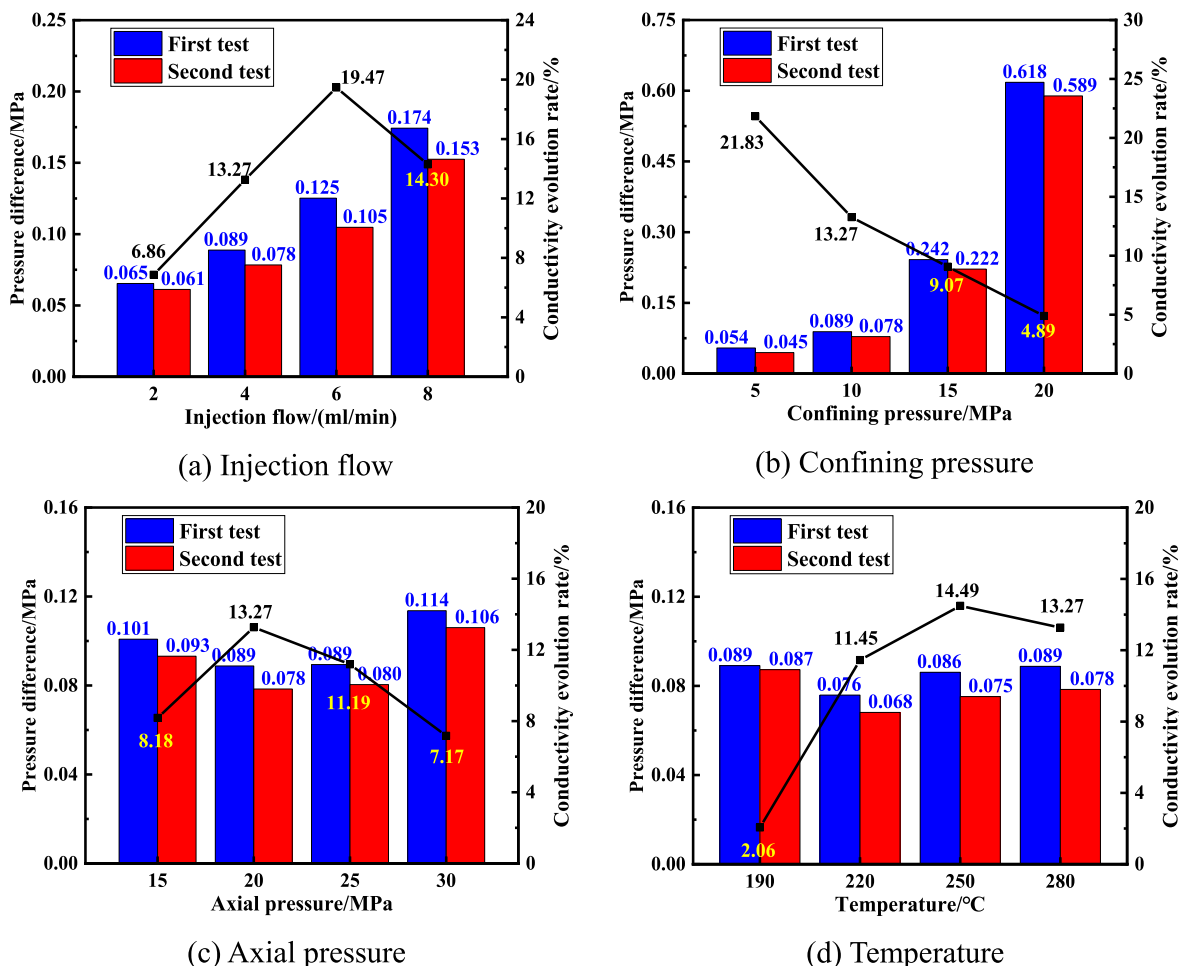


Fig. 16. Comparison of results before the first and the second experiment.

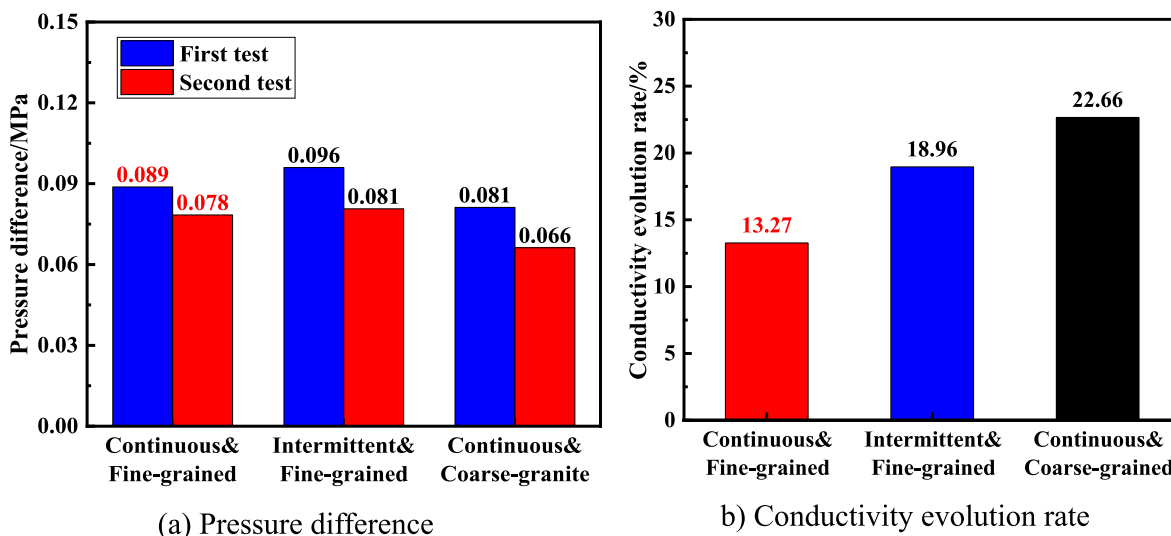


Fig. 17. Comparison of results before the first and second experiments.

Yu Shi: Formal analysis, Investigation, Resources, Writing – review & editing. **Xianzhi Song:** Conceptualization, Resources, Writing – original draft, Writing – review & editing. **Wei Wu:** Conceptualization, Writing – review & editing. **Guofeng Song:** Data curation, Writing – original draft. **Shuang Li:** Data curation.

Declaration of competing interest

The authors declare that they have no known competing financial interests or personal relationships that could have appeared to influence the work reported in this paper.

Data availability

Data will be made available on request.

Acknowledgments

The authors would like to acknowledge the National Natural Science Foundation of China (Grant No. 52104034, 52374010), the Major Program of the National Natural Science Foundation of China (Grant No. 52192624), New Interdisciplinary Discipline Cultivation Fund of Southwest Jiaotong University (Grant No. 2682023ZTPY030, 2682022KJ034), the China Scholarship Council (Grant No. 202206440098).

References

- Ji JY, Song XZ, Song GF, Xu FQ, Shi Y, Lv ZH, et al. Study on fracture evolution model of the enhanced geothermal system under thermal-hydraulic-chemical-deformation coupling. *Energy* 2023;269:126604.
- Song GF, Song XZ, Li GS, Shi Y, Wang GS, Ji JY, et al. An integrated multi-objective optimization method to improve the performance of multilateral-well geothermal system. *Renew Energy* 2021;172:1233–49.
- Zhang W, Wang CG, Guo TK, He JY, Zhang L, Chen SJ, et al. Study on the cracking mechanism of hydraulic and supercritical CO₂ fracturing in hot dry rock under thermal stress. *Energy* 2021;221:119886.
- Yang RY, Wang YY, Song GF, Shi Y. Fracturing and thermal extraction optimization methods in enhanced geothermal systems. *Adv Geo-Energy Res* 2023;9(2):136–40.
- Gong FC, Guo TK, Sun W, Li ZM, Yang B, Chen YM, et al. Evaluation of geothermal energy extraction in Enhanced Geothermal System (EGS) with multiple fracturing horizontal wells (MFHW). *Renew Energy* 2020;151:1339–51.
- Sun ZX, Jiang CY, Wang XG, Lei QH, Jourde H. Joint influence of in-situ stress and fracture network geometry on heat transfer in fractured geothermal reservoirs. *Int J Heat Mass Tran* 2020;149:119216.
- Zhao YS, Feng ZJ, Feng ZC, Yang D, Liang WG. THM (Thermo-hydro-mechanical) coupled mathematical model of fractured media and numerical simulation of a 3D enhanced geothermal system at 573 K and buried depth 6000–7000 M. *Energy* 2015;82:193–205.
- Song GF, Song XZ, Xu FQ, Li GS, Shi Y, Ji JY. Contributions of thermo-poroelastic and chemical effects to the production of enhanced geothermal system based on thermo-hydro-mechanical-chemical modeling. *J Clean Prod* 2022;377:134471.
- Aliyu MD, Finkbeiner T, Chen HP, Archer RA. A three-dimensional investigation of the thermoelastic effect in an enhanced geothermal system reservoir. *Energy* 2023; 262:125466.
- Guo TK, Zhang YL, Zhang W, Niu BL, He JY, Chen M, et al. Numerical simulation of geothermal energy productivity considering the evolution of permeability in various fractures. *Appl Therm Eng* 2022;201:117756.
- Xu FQ, Shi Y, Song XZ, Li GS, Song ZH, Li S. The characteristics and laws of fracture damage in the long-term production process of high-temperature geothermal resources. *Rock Mech Rock Eng* 2023;56:275–99.
- AbuAisha M, Loret B. Influence of hydraulic fracturing on impedance and efficiency of thermal recovery from HDR reservoirs. *Geomech Energy Envir* 2016; 7:10–25.
- Lei QH, Doonechaly NG, Tsang CF. Modelling fluid injection-induced fracture activation, damage growth, seismicity occurrence and connectivity change in naturally fractured rocks. *Int J Rock Mech Min* 2021;138:104598.
- Anyim K, Gan Q. Fault zone exploitation in geothermal reservoirs: production optimization, permeability evolution and induced seismicity. *Adv Geo-Energy Res* 2020;4(1):1–12.
- Demirdag S. Effects of freezing-thawing and thermal shock cycles on physical and mechanical properties of filled and unfilled travertine. *Construct Build Mater* 2013; 47:1395–401.
- Hall K, Thorn E. Thermal fatigue and thermal shock in bedrock: an attempt to unravel the geomorphic processes and products. *Geomorphology* 2014;206:1–13.
- Kumari WGP, Ranjith PG, Perera MSA, Chen BK, Abdulagatov IM. Temperature-dependent mechanical behaviour of Australian Strathbogie granite with different cooling treatments. *Eng Geol* 2017;229:31–44.
- Wu XG, Huang ZW, Cheng Z, Zhang SK, Song HY, Zhao X. Effects of cyclic heating and LN₂-cooling on the physical and mechanical properties of granite. *Appl Therm Eng* 2019;156:99–110.
- Zhang F, Zhao JJ, Hu DW, Skoczylas F, Shao JF. Laboratory investigation on physical and mechanical properties of granite after heating and water-cooling treatment. *Rock Mech Rock Eng* 2018;51:677–94.
- Kranz RL. Microcracks in rocks: a review. *Tectonophysics* 1983;100(1–3):449–80.
- Guo TY, Wong LNY, Wu ZJ. Microcracking behavior transition in thermally treated granite under mode I loading. *Eng Geol* 2021;282:105992.
- Nasseria MHB, Schubnela A, Young RP. Coupled evolutions of fracture toughness and elastic wave velocities at high crack density in thermally treated westerly granite. *Int J Rock Mech Min* 2007;44(4):601–16.
- Li N, Zhang SC, Ma XF, Zou YS, Li SH, Zhang ZP. Thermal effect on the evolution of hydraulic fracture conductivity: an experimental study of enhanced geothermal system. *J Petrol Sci Eng* 2020;187:106814.
- Wu QH, Weng L, Zhao YL, Guo BH, Luo T. On the tensile mechanical characteristics of fine-grained granite after heating/cooling treatments with different cooling rates. *Eng Geol* 2019;253:94–110.
- Freire-Lista DM, Fort R, Varas-Muriel MJ. Thermal stress-induced microcracking in building granite. *Eng Geol* 2016;206:83–93.
- Vázquez P, Shushakova V, Gómez-Heras M. Influence of mineralogy on granite decay induced by temperature increase: experimental observations and stress simulation. *Eng Geol* 2015;189:58–67.
- Cowie S, Walton G. The effect of mineralogical parameters on the mechanical properties of granitic rocks. *Eng Geol* 2018;240:204–25.
- Yang FJ, Wang GL, Hu DW, Liu YG, Zhou H, Tan XF. Calibrations of thermo-hydro-mechanical coupling parameters for heating and water-cooling treated granite. *Renew Energy* 2021;168:544–58.

- [29] Zhang B, Tian H, Dou B, Zheng J, Chen J, Zhu ZN, et al. Macroscopic and microscopic experimental research on granite properties after high-temperature and water-cooling cycles. *Geothermics* 2019;93:102079.
- [30] Zhu ZN, Kempka T, Ranjith PG, Tian H, Jiang GS, Dou B, et al. Changes in thermomechanical properties due to air and water cooling of hot dry granite rocks under unconfined compression. *Renew Energy* 2021;170:562–73.
- [31] Shu B, Zhu RJ, Elsworth D, Dick J, Liu S, Tan JQ, et al. Effect of temperature and confining pressure on the evolution of hydraulic and heat transfer properties of geothermal fracture in granite. *Appl Energy* 2020;272:115290.
- [32] Shu B, Wang YM, Zhu RJ, Liu LL, Tan JQ, Dick J. Experimental study of the heat transfer characteristics of single geothermal fracture at different reservoir temperature and in situ stress conditions. *Appl Therm Eng* 2022;207:118195.
- [33] Zhang P, Zhang YJ, Huang YB, Xia Y. Experimental study of fracture evolution in enhanced geothermal systems based on fractal theory. *Geothermics* 2022;102:102406.
- [34] Caulk RA, Ghazanfari E, Perdril JN, Perdril N. Experimental investigation of fracture aperture and permeability change within Enhanced Geothermal Systems. *Geothermics* 2016;62:12–21.
- [35] Shu B, Zhu RJ, Tan JQ, Zhang SH, Liang M. Evolution of permeability in a single granite fracture at high temperature. *Fuel* 2019;242:12–22.
- [36] Shi Y, Song XZ, Li JC, Wang GS, Yulong FX, Geng LD. Analysis for effects of complex fracture network geometries on heat extraction efficiency of a multilateral-well enhanced geothermal system. *Appl Therm Eng* 2019;159:113828.
- [37] Chen SW, Yang CH, Wang GB. Evolution of thermal damage and permeability of Beishan granite. *Appl Therm Eng* 2017;110:1533–42.
- [38] Srinivasan V, Hasainar H, Singh TN. Experimental study on failure and fracturing attributes of granite after thermal treatments with different cooling conditions. *Eng Geol* 2022;310:106867.
- [39] Breede K, Dzebisashvili K, Liu X, Falcone G. A systematic review of enhanced (or engineered) geothermal systems: past, present and future. *Geoth Energy* 2013;1(1):4.
- [40] Liu G, Wang G, Zhao Z, Ma F. A new well pattern of cluster-layout for deep geothermal reservoirs: case study from the Dezhou geothermal field, China. *Renew Energy* 2020;155:484–99.
- [41] Scientific platform serving for statistics professional. SPSSPRO; 2021. Version 1.0.11 [Online Application Software]. Retrieved from, <https://www.spsspro.com>.
- [42] Azzeh M, Neagu D, Cowling PI. Fuzzy grey relational analysis for software effort estimation. *Empir Software Eng* 2010;15(1):60–90.
- [43] Song Q, Shepperd M, Mair C. Using grey relational analysis to predict software effort with small data sets. *Proceedings of the 11th International Symposium on Software Metrics (METRICS'05)* 2005:35–45.